Ocean Modelling 122 (2018) 26–35

Contents lists available at ScienceDirect

Ocean Modelling

journal homepage: www.elsevier.com/locate/ocemod

Idealised modelling of ocean circulation driven by conductive and hydrothermal fluxes at the seabed

Jowan M. Barnes[*,a,b], Miguel A. Morales Maqueda[a], Jeff A. Polton[b], Alex P. Megann[c]

[a] School of Natural and Environmental Sciences, Newcastle University, Newcastle Upon Tyne NE1 7RU, United Kingdom
[b] National Oceanography Centre, Joseph Proudman Building, 6 Brownlow Street, Liverpool L3 5DA, United Kingdom
[c] National Oceanography Centre, Southampton University Waterfront Campus, European Way, Southampton SO14 3ZH, United Kingdom

ARTICLE INFO

Keywords:
Abyssal circulation
Ocean modelling
Hydrothermal
Geothermal heating
Heat flux

ABSTRACT

Geothermal heating is increasingly recognised as an important factor affecting ocean circulation, with modelling studies suggesting that this heat source could lead to first-order changes in the formation rate of Antarctic Bottom Water, as well as a significant warming effect in the abyssal ocean. Where it has been represented in numerical models, however, the geothermal heat flux into the ocean is generally treated as an entirely conductive flux, despite an estimated one third of the global geothermal flux being introduced to the ocean via hydrothermal sources.

A modelling study is presented which investigates the sensitivity of the geothermally forced circulation to the way heat is supplied to the abyssal ocean. An analytical two-dimensional model of the circulation is described, which demonstrates the effects of a volume flux through the ocean bed. A simulation using the NEMO numerical general circulation model in an idealised domain is then used to partition a heat flux between conductive and hydrothermal sources and explicitly test the sensitivity of the circulation to the formulation of the abyssal heat flux. Our simulations suggest that representing the hydrothermal flux as a mass exchange indeed changes the heat distribution in the abyssal ocean, increasing the advective heat transport from the abyss by up to 35% compared to conductive heat sources. Consequently, we suggest that the inclusion of hydrothermal fluxes can be an important addition to course-resolution ocean models.

1. Introduction

Geothermal fluxes through the ocean floor have only recently been considered as a significant factor influencing ocean circulation. The global average of the geothermal heat flux into the oceans is estimated by Davies and Davies (2010) to be 105.4 mW m^{-2}. At first glance it seems that neglecting these fluxes could be justified, as net heat fluxes at the surface can be a thousand times greater in magnitude. However, this is not an entirely meaningful comparison. The conductive component of the geothermal heat flux is always directed upwards (e.g. Adcroft et al., 2001; Hofmann and Morales Maqueda, 2009; Emile-Geay and Madec, 2009), whereas the surface fluxes can be positive or negative, leading to cancellations on a global scale. Additionally, the dense water masses acted upon by geothermal fluxes are rarely in contact with the surface of the ocean. The surface area of outcropping Antarctic Bottom Water, for example, is about one thousand times less than the seabed contact area, thus making surface integrals of heat fluxes at the upper and lower boundaries comparable (Emile-Geay and Madec, 2009).

An increasing interest in the impact of geothermal heating on the large scale circulation in recent years has led to the process being modelled at the global scale. It had previously been studied at regional and basin scales (e.g. Stommel, 1982; Joyce and Speer, 1987; Speer, 1989; Thompson and Johnson, 1996), but the companion papers of Adcroft et al. (2001) and Scott et al. (2001) were the first to consider geothermal heat fluxes as an influence on the global circulation. Their modelling experiments, using a uniform seabed heat flux of 50 mW m^{-2}, showed average abyssal temperature rising by 0.3 °C and a 25% increase in the Pacific meridional overturning. This result is reinforced by consistent findings in the experiments of Hofmann and Morales Maqueda (2009), Emile-Geay and Madec (2009), Urakawa and Hasumi (2009), Mashayek et al. (2013) and Downes et al. (2016). Hofmann and Morales Maqueda (2009) used spatially varying geothermal heat fluxes based on the dataset of Pollack et al. (1993) to obtain an average abyssal temperature rise of about 0.4 °C and a 33% increase in the formation rate of Antarctic Bottom Water. Emile-Geay and Madec (2009) followed a different method, using the formula of Stein and Stein (1992) relating heat flow to crustal age and the high-

* Corresponding author at: School of Natural and Environmental Sciences, Newcastle University, Newcastle Upon Tyne NE1 7RU, United Kingdom.
E-mail address: j.m.barnes2@newcastle.ac.uk (J.M. Barnes).

https://doi.org/10.1016/j.ocemod.2017.12.005
Received 26 August 2017; Received in revised form 18 December 2017; Accepted 21 December 2017
Available online 23 December 2017
1463-5003/ © 2017 Published by Elsevier Ltd.

resolution dataset of crustal age from Müller et al. (1997), to produce similar results. In another modelling study (Piecuch et al., 2015) found that inclusion of geothermal heating raised the global mean sea level trend, showing that its effects can be seen throughout the entire water column.

The geothermal heat flux into the ocean has two components: conductive and advective (or hydrothermal). There is compelling modelling evidence to suggest that geothermal heating is an important contributor to global circulation, but all of the experiments mentioned above employ an entirely conductive heat flux. This is a potentially serious shortcoming since hydrothermal fluxes have a far from negligible contribution to the geothermal heating of the global ocean. The global flow of hydrothermal fluids in and out of the crust has been estimated at up to 0.35 Sv (Elderfield and Schultz, 1996). This is equivalent to one third of the global ocean's freshwater input from rivers and surface runoff, a process which, like hydrothermal activity, has a strong buoyancy signature. Towards the young crust on the flanks of mid-ocean ridges there is a discrepancy between predicted and observed geothermal heating (Anderson and Hobart, 1976), known as the heat flow anomaly. As the observational methods measure conductive heat, this discrepancy can be explained by the co-existence of conductive heating and hydrothermal circulations, the latter being dominant in areas where the crust is highly permeable and pathways exist which allow water to flow in and out of the ocean through the seabed (e.g. Harris and Chapman, 2004). Stein and Stein (1994) compare the heat flow model of Stein and Stein (1992) to observations and, by studying the heat flow anomaly, conclude that more than half of the geothermal heat flux through 10 million year old crust is advective in nature (i.e. hydrothermal) and that the proportion increases as the crust becomes younger. They estimate that 34% of global heat flow is hydrothermal, which is in agreement with the earlier estimate of Sclater et al. (1980) that one third of the total heat entering the ocean from below does so hydrothermally. It seems reasonable to conjecture that this amount of advective flux must have an impact on the abyssal circulation different from that of a purely conductive heat flux.

The purpose of the work presented here is to gain understanding, in a modelling context, of the importance of hydrothermal flows in geothermally driven circulations at the scale of an ocean basin. To this end, we have introduced a physically consistent formulation of hydrothermal fluxes in the primitive equation ocean model NEMO (Madec, 2008) and conducted a number of numerical experiments to characterise the relative importance of hydrothermal and conductive heat fluxes. To our knowledge, this is the first time such hydrothermal flows have been implemented in an ocean circulation model of this type.

The rest of the paper is organised as follows. In Section 2, we present an analytical model used to assess the impact of a neutrally buoyant flux through the seabed on an otherwise motionless bottom layer. We then move on to more complex, but still idealised, formulations that include heat fluxes in Section 3. In this section, we describe the implementation of conductive and hydrothermal fluxes in the NEMO model and how the net geothermal flux is partitioned between the two. In Section 4 results from a series of numerical experiments are presented and interpreted with a focus on the differences between the two extremes, where the heat source is either entirely conductive or entirely hydrothermal in nature. In Section 5, we discuss the findings of our experiments, their relevance to the real world and what implications our results may have on future modelling.

2. Motivation: circulation driven by vertical volume fluxes through the seabed

Mass or volume flux through the seabed has not been implemented in ocean modelling to date, so it is important to detail this process here. We take a simple first look at the effects of adding a flux of volume (imposed as a velocity per unit length) through the seabed using the linearised steady state shallow water equations. We assume that all properties in the y-direction are constant, so $\frac{\partial}{\partial y} = 0$. In the vertical, $z = 0$ coincides with a flat seabed and the undisturbed free surface of the abyssal mixed layer is located at $z = \mathscr{H}$, so that the thickness of the abyssal mixed layer is in general $h(x) = \mathscr{H} + \eta(x)$, where $\eta(x)$ is a small perturbation.

The system is then described by the frictional geostrophic equations

$$-fv = -Ru - g'\frac{\partial h}{\partial x} \tag{1a}$$

$$fu = -Rv \tag{1b}$$

$$\frac{\partial u}{\partial x} + \frac{\partial w}{\partial z} = 0, \tag{1c}$$

with boundary conditions

$$w(x, h(x)) = u\frac{\partial h}{\partial x} \tag{2a}$$

$$w(x, 0) = w_b \tag{2b}$$

$$u, \eta \to 0 \quad \text{as } x \to -\infty, \tag{2c}$$

where u, v and w are the velocities in the x-, y- and z-directions, respectively. The constants R and g' are a Rayleigh friction coefficient and the reduced gravity in the layer, respectively. The prescribed function $w_b(x)$ describes the distribution of the vertical fluid velocities through the seabed boundary, and should be constructed so as to ensure that the domain conserves its volume (i.e. that the integral of w_b across the whole domain is zero).

Since the problem is linear, we arrive at the solutions for u, v, h and w being

$$u(x) = \frac{\int_{-\infty}^{x} w_b(\xi)\,\mathrm{d}\xi}{h(x)} \tag{3a}$$

$$v(x) = -\frac{f}{R}u(x) \tag{3b}$$

$$h(x) = \sqrt{\mathscr{H}^2 - \frac{2(f^2 + R^2)}{Rg'}\int_{-\infty}^{x}\left(\int_{-\infty}^{\zeta} w_b(\xi)\,\mathrm{d}\xi\right)\mathrm{d}\zeta} \tag{3c}$$

$$w(x, z) = w_b(x) - \left(w_b(x) + \frac{(f^2 + R^2)u^2}{Rg'}\right)\frac{z}{h}. \tag{3d}$$

This solution shows that the flow, u, along the x direction results from the horizontal divergence caused by the discharge and recharge of water through the seabed (3a), while the horizontal cross flow, v, is a balance between the components of friction and the Coriolis force in the y direction (3b). Since we assume there is no stratification within the bottom mixed layer, the horizontal flow is vertically uniform (from the Taylor–Proudman theorem) and the vertical velocity varies linearly from its value at the seabed w_b to that at the top of the mixed layer, which is in general non-zero to ensure that there is no flow across this interface. The shape of the interface itself is determined by the shape of the velocity function w_b.

To illustrate the resulting solutions, we choose the function w_b to be symmetric, with an upwards flow centred at $x = 0$ flanked by two areas of downward flow. This is designed to mimic a hydrothermal vent field surrounded by porous seabed through which the water re-enters the crust. To avoid discontinuity in the boundary function and ensure volume is conserved, we set

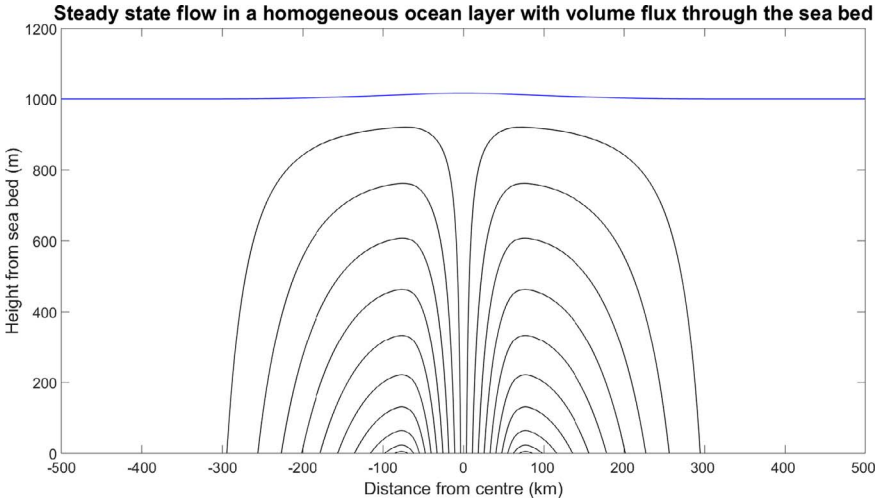

Fig. 1. Analytical flow. The flow lines of a circulation driven by a volume flux w_b (defined by the piecewise function given in the text, with a central upwelling and surrounding downwelling zones) and with the free surface of the 1000 m thick ocean layer plotted at the top.

$$w_b = \begin{cases} w_0 \frac{L_1}{L_2 - L_1} \sin\left(\frac{\pi(x+L_1)}{L_2 - L_1}\right) & \text{if } -L_2 \le x < -L_1 \\ w_0 \cos\left(\frac{\pi x}{2L_1}\right) & \text{if } -L_1 \le x \le L_1 \\ -w_0 \frac{L_1}{L_2 - L_1} \sin\left(\frac{\pi(x-L_1)}{L_2 - L_1}\right) & \text{if } L_1 < x \le L_2 \\ 0 & \text{otherwise,} \end{cases} \quad (4)$$

where w_0 is the maximum velocity of the discharge, chosen to be 10^{-7} m s^{-1}. In line with the numerical simulations that will be presented in Section 3, the distances from the centre of the discharge L_1 and L_2 are chosen to be 69 km and 347 km ($\frac{5}{8}$ and $\frac{25}{8}$ degrees of latitude, respectively, near the equator) and $\mathscr{H} = 1000$ m. We also choose $R = 10^{-10}$ s^{-1}, $f = 7.63 \times 10^{-6}$ s^{-1} and $g' = 0.029$ m s^{-2}. Using these parameters we obtain a fountain-shaped overturning flow, shown in Fig. 1, with an upward displacement of the layer surface above the water discharge area. The discharged flow extends vertically through the entire unstratified layer which, in our example, is meant to represent the mixed layer of the abyssal ocean.

3. Geothermally driven circulations with both conductive and hydrothermal heat fluxes

Having discussed the circulation which could arise from volume fluxes alone, we will now investigate the effects of adding heat into the system both through the hydrothermal fluxes (in which the temperature of the discharge is typically higher than that of the abyssal water) and via conduction. The calculations involved are far more complex than those above and thus require a numerical model. To this end, we have created a configuration of the NEMO (Nucleus for European Modelling of the Ocean) modelling framework (Madec, 2008) which allows the partitioning of the heat flux between conductive and hydrothermal input at the seabed. Our configuration uses a TVD (Total Variance Dissipation) advection scheme that implements the method of Zalesak (1979). Lateral eddy diffusion and transport are parameterised through isopycnic Redi (Redi, 1982) and Gent–McWilliams (Gent and McWilliams, 1990) diffusion with uniform diffusivities of 30 m^2 s^{-1} for both processes. This is smaller than lateral diffusivities that might be used higher up in the water column, but the abyssal currents are relatively small and we do not wish to have them masked by diffusive effect. A lower lateral diffusivity allows us to better observe the impacts of advective processes. In the vertical, we use a uniform diapycnal diffusivity of 1.2×10^{-5} m^2 s^{-1}, except when the water column becomes hydrostatically unstable, in which case the vertical diffusion is ramped up to 100 m^2 s^{-1} in order to parameterise vertical convection. The introduction of conductive fluxes through the seabed uses the paramaterisation of Emile-Geay and Madec (2009). Hydrothermal fluxes are formulated by prescribing a field of vertical velocities at the seabed, representing the net hydrothermal volume exchange per unit area between the oceanic crust and the abyssal ocean. These vertical velocities enter as a bottom boundary condition in the continuity equation, thus ensuring that volume is conserved (NEMO uses the Boussinesq approximation) and that the barotropic mode is solved correctly (we use the fully non-linear free surface formulation of the barotropic mode implemented in NEMO). The advective flux of hydrothermal properties (e.g. temperature and salinity) across the ocean bottom is calculated using an upstream transport approach, namely, waters flowing upwards from the crust into the ocean have prescribed properties, while waters flowing downwards into the crust leave the ocean with the properties of the deepest oceanic model cell at each horizontal location. The volume flux formulation was tested in an unstratified rectangular basin matching that of our analytical model. Solutions from the two were compared in order to verify that our new configuration operates as intended. Similar circulation patterns were created, and all three velocity fields showed the same general behaviour in both cases.

Our model configuration reflects the basic features of the Panama Basin in the equatorial east Pacific (Fig. 2). This basin is entirely enclosed below about 2000 m except for the saddle of the Carnegie Ridge, which does not extend deeper than 2500 m, and the Ecuador Trench, which allows water to be exchanged with the southern Pacific along the edge of the South American continental shelf at a depth of about 2700 m. Thus the abyssal Panama Basin is almost entirely isolated from the rest of the Pacific ocean. The region is of interest due to the known importance of geothermal heating in its circulation, as evidenced by several surveys of the region in the 1970s. The area has not been heavily studied since, but has recently become the focus for interdisciplinary research into interactions between the ocean and solid Earth. Observations suggest that vertical mixing in the basin is negligible (Laird, 1971), which would mean that the conditions in the abyss are mostly due to seabed processes. An estimate based on inflow measured at the Ecuador Trench gives a relatively fast vertical advection averaging 17 m yr^{-1} (Lonsdale, 1977). The renewal of bottom water in the basin requires a driving force, and calculations based on a theoretical heat flow driving the circulation are consistent with observations of the oxygen consumption rate (Laird, 1971; Detrick et al., 1974).

The idealised model domain is two-dimensional, in keeping with the previous analytical problems. This prevents extra complexities such as eddy formation, and allows us simpler solutions in this first step towards understanding the effects of differing heat fluxes. This is achieved in NEMO by using only one grid cell in the x-direction and applying cyclical boundary conditions. The resolution is $\frac{1}{8}^\circ$ (13.875 km)

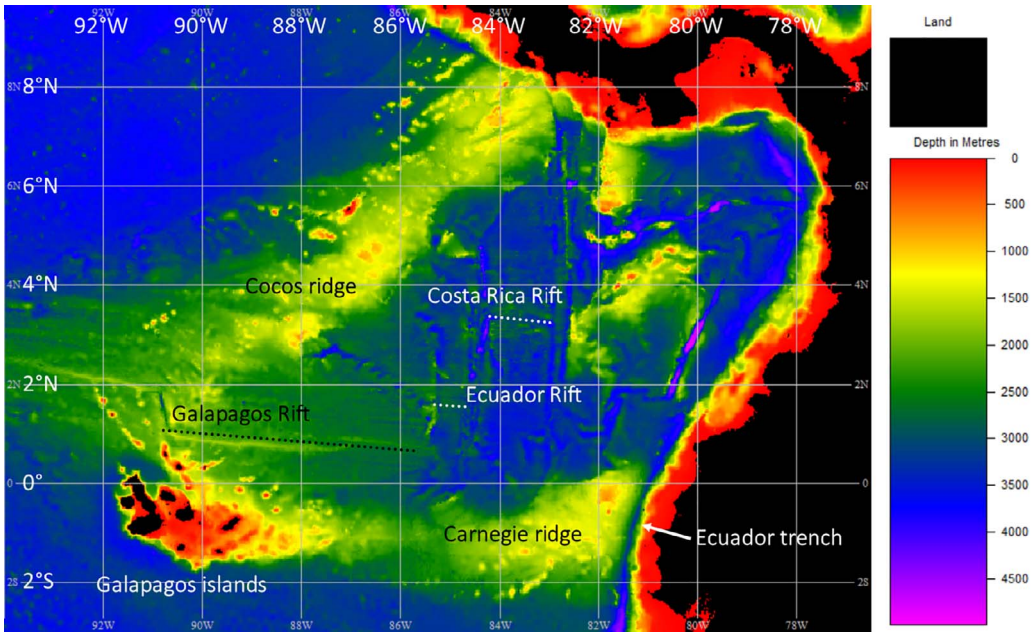

Fig. 2. Panama Basin map. A map of the Panama Basin, using bathymetry data from GEBCO (British Oceanographic Data Centre, 2015).

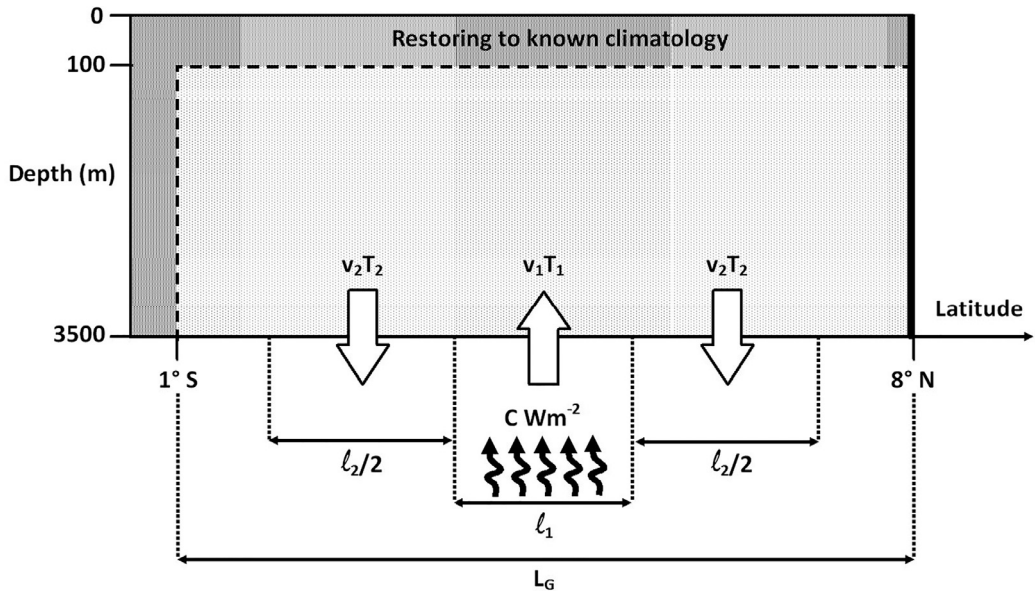

Fig. 3. Sketch of model domain. A sketch of the 2D model domain representing features of the Panama Basin, and the fluxes being applied through the seabed. The symmetrical basin used in some experiments is the same, but with a solid wall at 1° S and thus with no restoring at either side of the basin.

in the horizontal, spanning the region from 2° S to 8° N, and there are 60 vertical levels chosen to give greater resolution to the deepest parts of the ocean, ranging almost linearly from 10 m thick at the bottom of the domain to 100 m thick at the top. The configuration is designed to crudely represent a North–South cross section through the Panama Basin, as displayed in Fig. 3. The north side of the model domain is a solid wall, representing the coastline of Central America. At the other side, south of 1° S, the hydrography is restored with a time scale of one year to a climatological profile of temperature and salinity in the area taken from the World Ocean Atlas (Locarnini et al., 2013; Zweng et al., 2013). This relaxation tries to represent in a simple way the effects of the flow through the Ecuador Trench. Restoring is also used at the surface, in the top 100 m of the domain with a time scale of one month, as a proxy for surface heat and freshwater fluxes. This leaves the abyssal ocean in our model free to evolve in response to geothermal forcing and the restoring at the boundaries. In a preliminary set of experiments we show simulations in a symmetrical basin with a solid wall either side, to better compare the results with our analytical flow solution.

Heat fluxes are introduced into the ocean across an area of the seabed at the centre of the domain, distributed according to a cosine function as in the analytical model, influenced by the fact that more heat enters the abyssal ocean closer to the spreading centres of mid-ocean ridges such as those in the middle of the Panama Basin. At either side are areas of hydrothermal recharge which allow water to flow out of the system at such a rate as to conserve the total volume, just as in the analytical model. We apply an average total geothermal heat flux of G over the length of the domain, L_G. This is partitioned into a conductive heat flux of C applied over a length ℓ_1, and a hydrothermal flux with a given temperature and discharge velocity. A hydrothermal discharge with temperature T_1 and average velocity v_1 is applied over ℓ_1. The recharge occurs over a length ℓ_2 (half at either side of the discharge) with temperature T_2 being equal to that of the bottom water as calculated by the model averaged over the area of recharge, and average velocity $v_2 = -\frac{v_1 \ell_1}{\ell_2}$ in order to conserve volume. The heat fluxes H_1 and H_2 associated with the hydrothermal flows are $H_i = v_i T_i \rho c_p$, where ρ is a reference density and c_p is a specific heat capacity. We use

the values $\rho = 1035$ kg m^{-3} and $c_p = 4000$ J kg^{-1}K^{-1}. To have heating take place over the same width as a mid-ocean ridge, we choose $\ell_1 = \frac{5}{4}^\circ$ (10 grid cells, approximately 139 km). We choose $\ell_2 = 5^\circ$ (40 grid cells, 555 km), larger than ℓ_1 to ensure that the recharge velocity is less vigorous than the discharge.

In all our experiments we enforce $G = 105.4$ mW m^{-2}, based on the Davies and Davies (2010) global average heat flow value. This heat input is partitioned between hydrothermal and conductive fluxes by use of the term $0 \le \alpha_H \le 1$, a measure of the proportion of the heat flux which is introduced hydrothermally. Partitioning the heat flux in this way, and uniformly for the entire length of the seabed, gives us the relations

$$(1 - \alpha_H) G L_G = C \ell_1 \tag{5a}$$

$$\alpha_H G L_G = H_1 \ell_1 + H_2 \ell_2. \tag{5b}$$

The hydrothermal fluxes must be prescribed in the model either by their temperature T_1 or their discharge rate v_1 and then, to preserve the prescribed net heat flux, the unprescribed variable is calculated using either

$$v_1 = \frac{\alpha_H G L_G}{(T_1 - T_2)\ell_1 \rho c_p} \tag{6a}$$

$$\text{or} \quad T_1 = \frac{\alpha_H G L_G}{v_1 \ell_1 \rho c_p} + T_2. \tag{6b}$$

We have made the choice of prescribing T_1 as $T_1 = T_b + \Delta T$, where T_b is the average ocean bottom temperature over the discharge area and ΔT is a prescribed positive anomaly which we vary from one experiment to the next, thus allowing us to also explore a range of values of v_1 via (6a). For each temperature difference ΔT, a set of five simulations were run with $\alpha_H = 0, 0.25, 0.5, 0.75, 1$. The model was integrated until it reached a near-steady state at which the maximum temperature change below 2500 m was smaller than 0.001 °C over a decade.

4. Results

4.1. Symmetric experiments

Before embarking upon our main set of experiments, we carried out simulations with no lateral restoring as an intermediate step between our analytical model and the experiments inspired by the Panama Basin. The initial stratification in these experiments was as in the Panama Basin simulations and restoring was applied only at the surface. Solid boundaries are on both sides of the domain. The hydrothermal discharge and conductive heating were applied between 2.875°N and 4.125°N. Two experiments were run to near-steady state, one with a high-velocity purely hydrothermal flux ($\alpha_H = 1$, $\Delta T = 0.01$) and one with a purely conductive flux ($\alpha_H = 0$). The streamlines in Fig. 4 show that the two types of heat flux cause rather different circulations. The flow induced by the conductive flux (Fig. 4(a)) shows simple overturning cells where water that is heated and rises is replaced via a lateral flow. In the hydrothermal case (Fig. 4(b)) we see a fountain shape reminiscent of that seen in the analytical solutions, although with extra complexities introduced by the hydrothermal source including heat in addition to just volume. Indeed, while in the analytical study the horizontal flow is directed away from the discharge area at all depths, in the numerical simulations there is horizontal convergence as relatively cold water is advected towards the source area at depths below about 3000 m to replace the warmer water convecting upwards.

The upper extent of the main overturning circulations in each case is around 2600 m. This suggests that the upwelling water above the heat source reaches neutral buoyancy at the same depth in both cases, indicating little difference in the temperature of the water at that point. After reaching this maximum height, the flows spread outwards. The hydrothermal source induces a wider-reaching circulation, as the

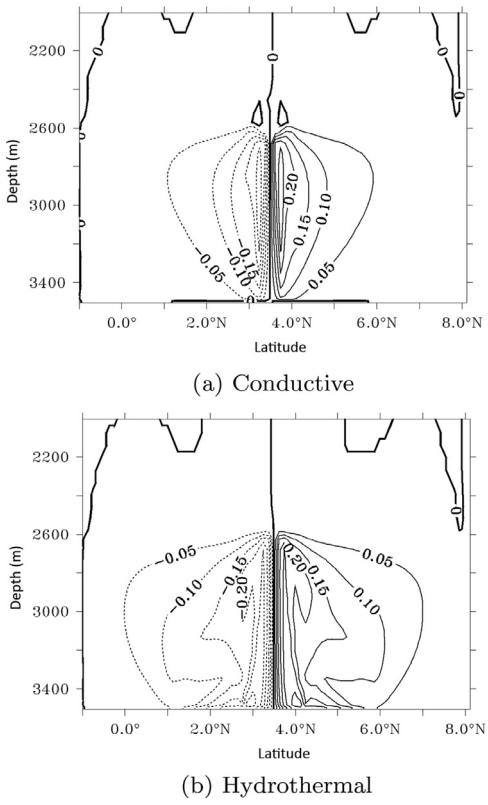

Fig. 4. Symmetrical streamlines. Streamlines for the symmetrical basin, in m^{2}s^{-1}, with (a) conductive ($\alpha_H = 0$) and (b) hydrothermal ($\alpha_H = 1$) fluxes.

downward flow at the bottom boundary causes streamlines to terminate in the recharge zones on the seabed rather than circulating back around to the centre again. In reality the hydrothermal circulation continues under the surface of the oceanic crust, outside of the model domain. Closer to the source, the streamlines in the hydrothermal case are drawn towards the centre before eventually ending up in the seabed. This suggests that the hydrothermal inflow is heating the surrounding abyssal water and causing a greater upwelling than can be balanced by the prescribed inflow alone. As in the conductive case, some water needs to flow in from the sides to replace that which becomes more buoyant and rises.

4.2. Panama Basin experiments

The only difference between the symmetrical experiments and our Panama Basin setup is in the lateral restoring field. These experiments implement restoring down one side to mimic the inflow through the Ecuador Trench, as shown schematically in Fig. 3. Our results show several differences in circulation and temperature distribution between experiments. The hydrothermal flux regime seems to be more effective at evacuating heat from the abyssal ocean than the conductive regime. As would be expected, this difference becomes more pronounced as the value of α_H increases and the heat flux becomes more dominated by its hydrothermal component. The evolution of the average temperature in the abyssal ocean varies fairly linearly with α_H, as is shown in Fig. 5.

Due to the formulation of our fluxes as described in Section 3, a lower temperature difference between the hydrothermal discharge and bottom waters necessitates a larger mass flux. The choice of ΔT makes a big difference to the impacts of a hydrothermal heat flux. Where $\Delta T = 10$°C, the conductive and hydrothermal cases are almost indistinguishable in both heat distribution and circulation dynamics. As ΔT decreases and the velocity of the discharge increases, much larger differences are seen between the two cases. The differences in the circulation and heat distribution are intrinsically linked, so where larger

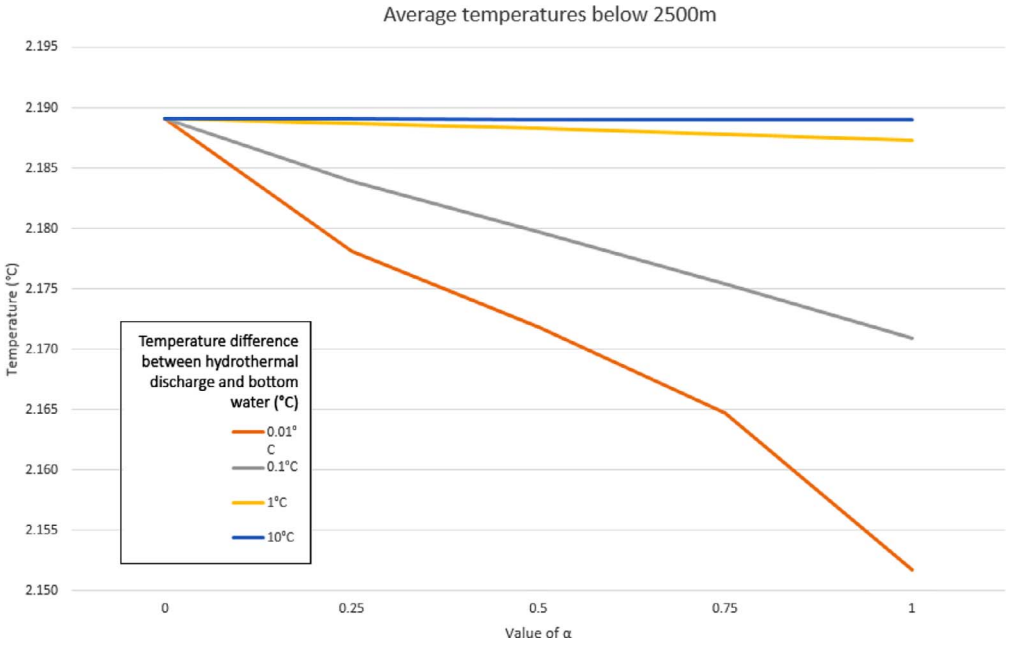

Fig. 5. Temperature graph. The average abyssal temperatures for hydrothermal flows with a range of temperature/velocity balances as α_H varies.

differences in the average abyssal temperature are seen in Fig. 5 we also see larger differences in the circulation. The comparisons we make throughout the rest of this section are between a purely conductive flux and a high velocity hydrothermal flux, the two extreme cases among our sets of experiments. The reality will lie somewhere between the two extremes, but this comparison allows us to clearly investigate the different effects these two types of heat flux have on the abyssal ocean.

The effect of applying a lateral restoring on the southern flank of the domain is the creation of an asymmetric circulation. On the north side of the basin where there is simply a wall, the abyssal ocean is well-mixed, but on the south side a strong stratification with slanted isotherms is maintained, as can be seen in Fig. 6. The area in which lateral restoring is applied does not appear in any of the figures, as it is not intended to represent any part of the interior of the basin, only to mimic the effects of flow through the Ecuador trench.

Looking at the distribution of temperature differences throughout the basin between the purely hydrothermal and the purely conductive cases (Fig. 6(e)), we find that, while the average temperature is lower in the former, the temperature is higher at the southern side of the basin near the seabed. This temperature difference of up to 0.3 °C occurs just above the southern recharge zone.

Plotting the streamlines of the two different flows helps us to understand how differences in circulation are linked to the different temperature distributions (Fig. 7). The effect of the lateral boundary restoring is seen again, with a strong circulation maintained throughout the southern half of the basin and comparatively little flow at the northern side. The hydrothermal fluxes also produce a relatively strong horizontal flow from the area of discharge to the area of recharge along the very bottom level of the ocean domain. The conductive case is in contrast, exhibiting a weak horizontal flow in the other direction, i.e. towards the centre of the basin, as water from the sides replaces the warmer water which rises due to buoyancy.

Looking more closely at the heat flux throughout the water column, we can try to determine further effects of the two different processes of geothermal heating. By calculating different components of the heat flux, we can investigate more precisely how the geothermal fluxes alter heat exchanges through the ocean. Consider a slab of the domain comprised between the seabed and a depth $z = d$, and between 1° S (y_S) and 8° N (y_N) where there is no restoring. The rate of change in the total heat content, Q, for this slab is due to the contributions of several heat transport processes, as illustrated in Fig. 8. The main contributions are from geothermal heating (F_{geo}), lateral advection (F_{lat}), vertical advection (F_{adv}) and vertical diffusion (F_{dif}). The eddy parameterisation fluxes of the model are included when calculating the advection and diffusion. The residual is given the shorthand F_{res}, and includes all unaccounted for numerical contributions to $\partial Q/\partial t$ such as spurious dispersion from the model's TVD advection scheme which is not included in the method of calculating advection below. It also includes the effects of lateral diffusion, which were not of great importance to our analysis. We write the heat content relationship mathematically as

$$\frac{\partial Q}{\partial t} = F_{geo} + F_{lat} - F_{adv} - F_{dif} + F_{res}, \tag{7}$$

where

$$Q = \mu \int_0^d \int_{y_S}^{y_N} T(y, z)\, dy\, dz \tag{8a}$$

$$F_{geo} = G \tag{8b}$$

$$F_{lat} = \mu \int_0^d v(y_S, z) T(y_S, z)\, dz \tag{8c}$$

$$F_{adv} = \mu \int_{y_S}^{y_N} w(y, h) T(y, h)\, dy \tag{8d}$$

$$F_{dif} = \mu \int_{y_S}^{y_N} \kappa(y, h) \frac{\partial T(y, h)}{\partial z}\, dy. \tag{8e}$$

In the expressions above, $\mu = \frac{\rho c_p}{y_N - y_S}$ is the multiplication factor which ensures that these values are heat fluxes into the specified slab (with units of Wm^{-2}) to remain consistent with our model's prescribed boundary condition. Additionally, ρ is a reference density, c_p is heat capacity, T is temperature, G is average geothermal heat flux, v and w are meridional and vertical velocity, and κ is vertical diffusivity.

These calculations are performed at each level interface by changing the value of d. We then have information about the average heat fluxes of each type in slabs of increasing thickness. Fig. 9 compiles the information into depth profiles of the average heat fluxes from the seabed up to a given depth. We ignore data from above 500 m depth as the surface restoring distorts the results. We can see that the changes caused by altering the heat flux at the seabed are confined to the deep ocean, and that above 1500 m depth there is almost no difference between the hydrothermal and conductive cases. Importantly, the difference is also confined to the advective components of the heat flux,

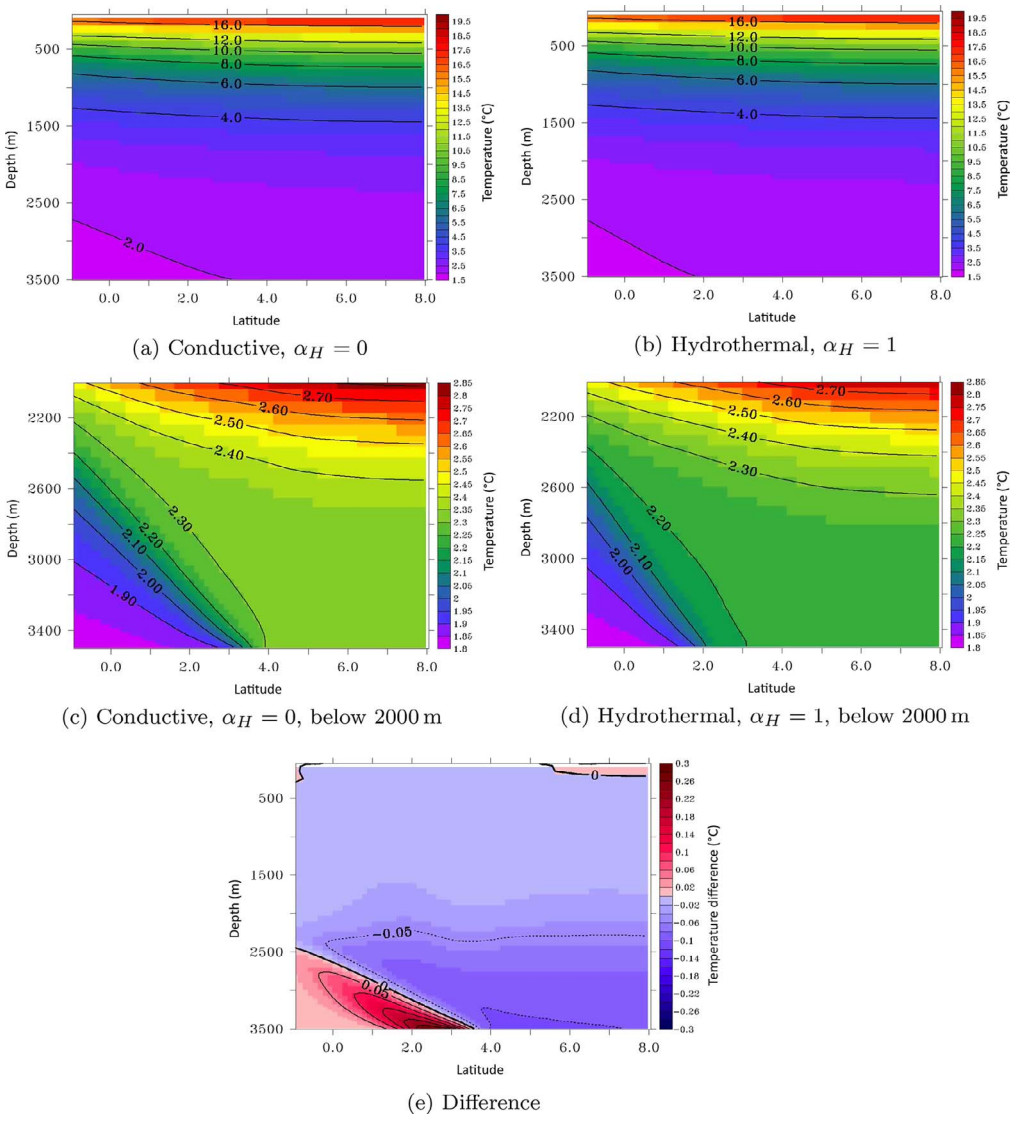

Fig. 6. Temperature fields. (a)–(d) Temperature fields for the full water column (a,b) and below 2000 m (c,d) in the two extreme cases ($\alpha_H = 0$, and $\alpha_H = 1$ with high velocity flow). (e) The difference between the two (hydrothermal minus conductive).

while changes in the vertical diffusive heat flux are negligible. Not unexpectedly, using a hydrothermal flux increases the strength of the advective components of the heat flux in the abyssal ocean. The vertical and lateral advective fluxes act to almost balance each other, irrespective of the value of α_H, with heat being evacuated from the abyss by the vertical advective flux and being replenished via lateral advection through the Ecuador trench. In the hydrothermal case the magnitude of the vertical advective flux in the abyssal ocean increases by up to 35% compared to the conductive case, being 21% greater on average between 2500 m depth and the seabed. The lateral advection increases by an even greater amount, up to 45% with an average change in the abyssal ocean of 28%. The strong vertical advection reaches a little further up the water column with a conductive source, so that above about 2350 m the advective fluxes are actually smaller in the hydrothermal case.

5. Discussion

From the experiments we have run, it appears that introducing a portion of the geothermal heat flux hydrothermally makes an important contribution to circulation in the abyssal ocean. Our analytical solution was the first indicator of the importance of these flows. Before even considering the effects of heating, the existence of a volume flux through the seabed, which has not been implemented in large-scale modelling before, contributes to the abyssal circulation. In the absence of other processes, the flow induced by these volume fluxes permeates the entire bottom mixed layer and causes a vertical displacement of its top interface.

In our numerical model we see many differences between the circulations, and the distribution and transportation of heat, induced by hydrothermal and conductive heat fluxes. With a hydrothermal flux as opposed to a conductive one, the advective heat transport in the abyssal ocean is increased by up to 35% in the vertical, and up to 45% laterally through the side of the basin. Due to our boundary conditions, this represents an increased flow though the Ecuador Trench. Meanwhile there is no appreciable change in the basin-averaged diffusive heat flux except at depths a few tens of metres above the seabed. So, in the purely hydrothermal simulation, we see the same effect as a conductive flux plus the additional advection caused by a velocity boundary condition. This was seen in our symmetrical model, which showed the streamlines of the hydrothermally driven flow moving in towards the heat source just as those of the conductive flow do, before turning back downwards to terminate in the seabed. In the Panama Basin setup, the increased vertical advection drives, through continuity, the increase in lateral advection through the side. It has previously been proposed, based on observational data, that flow through the Ecuador Trench is partly driven by upwelling in the basin interior caused by geothermal heating (Lonsdale, 1977). This theory agrees with the relationship we see

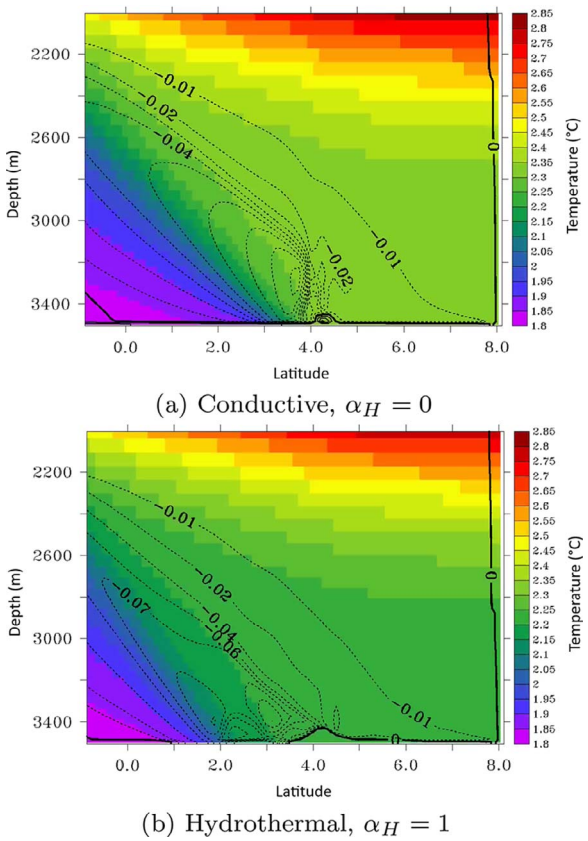

Fig. 7. Streamlines. Streamlines below 2000 m, in m^2s^{-1}, with (a) conductive and (b) hydrothermal fluxes, overlayed on the temperature fields.

between the vertical and lateral advective fluxes in our model.

When entering into this work we wanted to determine whether the use of hydrothermal, as opposed to purely conductive, fluxes in ocean models was a necessary addition to better represent the abyssal circulation, and under which circumstances it would be relevant if so. We have found that the impacts on circulation and heat distribution of a high-velocity hydrothermal flux are significant at basin scales in the abyssal ocean, but unlikely to make any noticeable difference in the upper ocean. So the usefulness of including these fluxes in ocean models very much depends on what one is interested in investigating. For future modelling of the abyssal circulation in the Panama Basin, it will be worth including hydrothermal boundary conditions in addition to conductive heat fluxes, since the Panama Basin has an average heat flux of 270 mW m^{-2}, calculated from the formula of Stein and Stein (1992) together with the crustal age data of Müller et al. (1997). This is about 2.5 times the global average used in our model, and so the differences between the two extreme model cases in the region could be even more significant than those we have seen in our results.

We previously noted that the abyssal temperature and circulation in our model results are sensitive to the choice of ΔT, the difference in temperature between the hydrothermal flow and the bottom water. The extreme case we focused on was $\Delta T = 0.01$ °C, but with larger values the differences between the circulations caused are less pronounced. While fluids from individual vents have been recorded at stable temperatures above 400 °C (Koschinsky et al., 2008), these are extremely small points when put in the context of a basin scale model. Since our lateral grid resolution is $\frac{1}{8}^\circ$ we must use values which represent the average ΔT over a large area. At this scale, taking into account the spacially sparce and scattered nature of hydrothermal venting and the fact that much of it occurs at much lower temperatures, a fraction of a degree Celcius seems a reasonable value for the average ΔT in the ocean.

Using a simple approach to this modelling was important in order to provide a clear first look at the processes, but it does come with some limitations. It is likely that areas of hydrothermal discharge and recharge are distributed in a far more disorderly manner than the symmetric boundary condition we implemented, creating far more complex flow patterns than in our simulations as competing regions of upward and downward velocity interact. The scales of realistic flows would likely be smaller in that case. Additionally, the conductive portion of the heat flux will be present throughout the entire basin rather than only at the centre, although the distribution of heat will be more heavily weighted towards the mid-ocean ridges, which is the justification for our idealised boundary condition.

6. Conclusion

Our idealised models have shown that the hydrothermal component of the global heat flux can affect the abyssal circulation in ways which a purely conductive heat flux cannot. Compared to the conductive case,

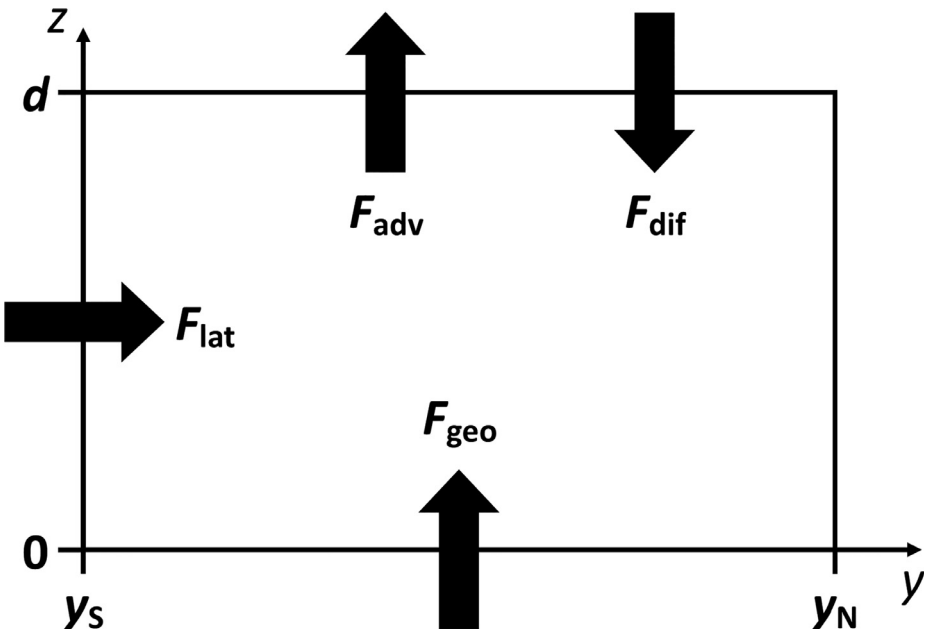

Fig. 8. Sketch of heat fluxes. Sketch showing the main contributions to the heat content of a slab of the abyssal ocean. We treat fluxes into the slab as positive and fluxes out of it as negative. F_{geo} is geothermal heating from below, F_{lat} is lateral advection, F_{adv} is vertical advection and F_{dif} is vertical diffusion.

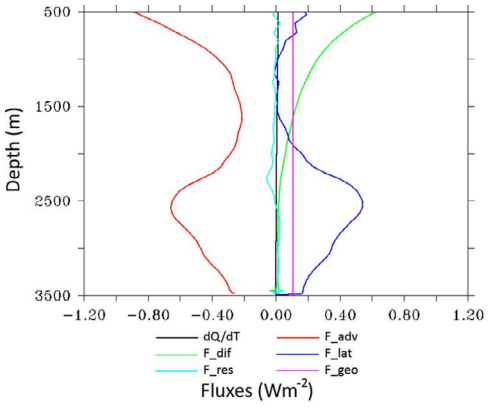

(a) Conductive, $\alpha_H = 0$

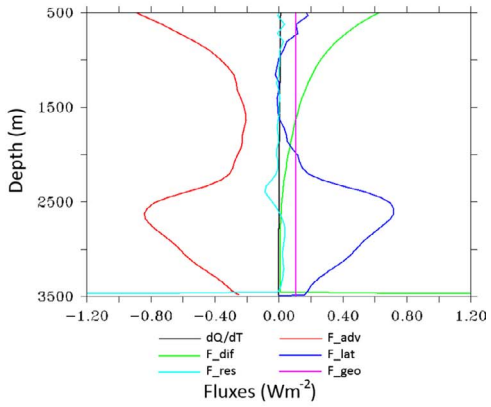

(b) Hydrothermal, $\alpha_H = 1$

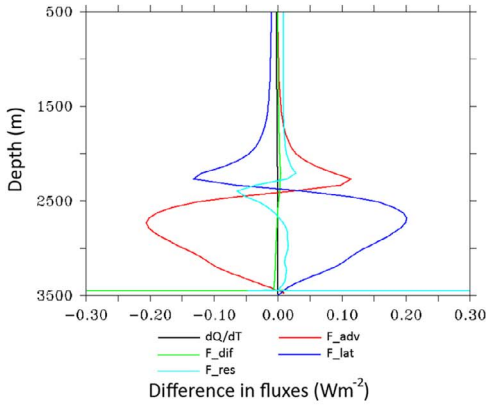

(c) Difference

Fig. 9. Heat flux depth profiles. (a) and (b) profiles of various components of the heat flux, in W m^{-2}, with (a) conductive and (b) hydrothermal fluxes. (c) The difference between the two (hydrothermal minus conductive).

the advective heat flux in our experiments is increased by up to 45% in the abyssal ocean. While the water below 2500 m is only slightly cooler on average, the heat is distributed differently such that there are localised patches which see temperatures change by up to 0.3 °C. It remains to be seen, however, whether the effects seen in our results will be present to the same degree of significance in a more realistic model. This is something we plan on investigating in further experiments with a full 3D regional model of the Panama Basin and using observational data from the area to help interpret the results. There could be complications in taking this method forward to more realistic modelling experiments, as creating realistic boundary conditions will not necessarily be a simple task. At coarser resolutions, the models of Stein and Stein (1992) will suffice, but for more detailed regional models observational data would be preferable. However, there are not many observations concerning the distribution of hydrothermal activity on the ocean floor, in particular how widespread or concentrated areas of discharge and recharge may be. Conducting a statistical study on the relative frequency of hydrothermal activity, Baker and German (2004) only had enough data to have a reasonable degree of confidence in their estimates for about 10% of the global ocean ridges. Nevertheless, hydrothermal boundary conditions will be considered in our future modelling studies of the area.

For more general usage, the importance of including the hydrothermal boundary condition will vary depending on the scales involved in the model, and the focus of the modelling project. For the upper ocean, we see no discernible difference between using conductive or hydrothermal heat fluxes, so it would not be a worthwhile addition for projects with their focus here. Deeper down, we see important differences in the heat distribution, but some of these occur only over small areas and may lose significance in lower resolution models. In particular our configuration, designed to emphasise changes in the abyss, contains a much finer resolution in the abyssal ocean than standard ocean circulation models. We would not expect to see such significant differences between the two types of heat flux when using standard vertical layers with resolutions often in the hundreds of metres in the abyss. The average abyssal temperature difference is under 0.04 °C, but our high resolution brings out areas where the temperature changes by up to 0.3 °C between the two cases. As such we would recommend a high vertical resolution in this part of the ocean for any experiments involving geothermal heating. At low resolutions, the introduction of hydrothermal boundary conditions will be less worthwhile.

Our findings have implications not only for the Panama Basin, but for other partially enclosed basins containing hydrothermal sources. Examples of such basins can be found across the globe, including the Scotia Sea, Cayman Trough, Red Sea, Sea of Japan and the Arctic Ocean. Simple models of the type we have been using could be adapted to take on the features of these other ocean basins and produce representative values for the components of their heat fluxes, quite possibly revealing higher advective transport in the same way as our results have for the Panama Basin.

It seems that the question of whether or not to include hydrothermal fluxes in models needs to be addressed on a case-by-case basis taking into account the above considerations. For any work with a focus on the abyssal ocean at a reasonably high resolution, it will certainly be a very useful addition to the modelling process.

Acknowledgements

This work is part of a major interdisciplinary NERC-funded collaboration entitled ‘Oceanographic and Seismic Characterisation of heat dissipation and alteration by hydrothermal fluids at an Axial Ridge’ (OSCAR), led by Richard Hobbs of Durham University.

The authors of this work have multiple funding sources. J M Barnes was supported by a NERC studentship (NE/JS00227/1) via the National Oceanography Centre and Durham University; M A Morales Maqueda and A P Megann by the OSCAR project (NE/I022868/1); J A Polton by FASTNEt (NE/I030259/1) and PycnMix (NE/L003325/1).

References

Adcroft, A., Scott, J.R., Marotzke, J., 2001. Impact of geothermal heating on the global ocean circulation. Geophys. Res. Lett. 28 (9), 1735–1738.

Anderson, R.N., Hobart, M.A., 1976. The relation between heat flow, sediment thickness, and age in the eastern pacific. J. Geophys. Res. 81 (17), 2968–2989.

Baker, E.T., German, C.R., 2004. On the global distribution of hydrothermal vent fields. In: German, C.R., Lin, J., Parson, L.M. (Eds.), Mid-Ocean Ridges. American Geophysical Union, Washington, D.C., pp. 245–266. http://dx.doi.org/10.1029/148GM10.

British Oceanographic Data Centre, The GEBCO_2014 Grid, version 20141103, http://www.gebco.net, 2015.

Davies, J.H., Davies, D.R., 2010. Earth’S surface heat flux. Solid Earth 1 (1), 5.

Detrick, R.S., Mudie, J.D., Williams, D.L., Sclater, J.G., 1974. The galapagos spreading centre: bottom-water temperatures and the significance of geothermal heating. Geophys. J. R. Astron. Soc. 38 (3), 627–637.
Downes, S.M., Hogg, A.M., Griffies, S.M., Samuels, B.L., 2016. The transient response of southern ocean circulation to geothermal heating in a global climate model. J. Clim. 29 (16), 5689–5708.
Elderfield, H., Schultz, A., 1996. Mid-ocean ridge hydrothermal fluxes and the chemical composition of the ocean. Annu. Rev. Earth Planet Sci. 24, 191–224.
Emile-Geay, J., Madec, G., 2009. Geothermal heating, diapycnal mixing and the abyssal circulation. Ocean Sci. 5 (2), 203–217.
Gent, P.R., McWilliams, J.C., 1990. Isopycnal mixing in ocean circulation models. J. Phys. Oceanogr. 20 (1), 150–155.
Harris, R.N., Chapman, D.S., 2004. Deep-seated oceanic heat flux, heat deficits, and hydrothermal circulation, in Hydrology of the Oceanic Lithosphere. pp. 311–336. https://www.gebco.net/data_and_products/gridded_bathymetry_data/documents/gebco_2014.pdf.
Hofmann, M., Morales Maqueda, M.A., 2009. Geothermal heat flux and its influence on the oceanic abyssal circulation and radiocarbon distribution. Geophys. Res. Lett. 36 (3), L03603. http://dx.doi.org/10.1029/2008GL036078.
Joyce, T.M., Speer, K.G., 1987. Modeling the large-scale influence of geothermal sources on abyssal flow. J. Geophys. Res. Oceans 92 (C3), 2843–2850.
Koschinsky, A., Garbe-Schönberg, D., Sander, S., Schmidt, K., Gennerich, H.-H., Strauss, H., 2008. Hydrothermal venting at pressure-temperature conditions above the critical point of seawater, 5°s on the mid-atlantic ridge. Geology 36 (8), 615–618.
Laird, N.P., 1971. Panama basin deep water properties and circulation. J. Mar. Res. 29 (3), 226–234.
Locarnini, R.A., et al., 2013. World Ocean Atlas 2013, Volume 1: Temperature. NOAA Atlas NESDIS 73.
Lonsdale, P., 1977. Inflow of bottom water to the panama basin. Deep Sea Res. 24 (12), 1065–1101.
Madec, G., 2008. NEMO Ocean Engine. No. 27. Note du Pôle de modélisation, Institut Pierre-Simon Laplace (IPSL), France, ISSN No. 1288–1619.
Mashayek, A., Ferrari, R., Vettoretti, G., Peltier, W., 2013. The role of the geothermal heat flux in driving the abyssal ocean circulation. Geophys. Res. Lett. 40 (12), 3144–3149.
Müller, R.D., Roest, W.R., Royer, J.-Y., Gahagan, L.M., Sclater, J.G., 1997. Digital isochrons of the world's ocean floor. J. Geophys. Res. Solid Earth 102 (B2), 3211–3214.
Piecuch, C.G., Heimbach, P., Ponte, R.M., Forget, G., 2015. Sensitivity of contemporary sea level trends in a global ocean state estimate to effects of geothermal fluxes. Ocean Modell. 96, 214–220.
Pollack, H.N., Hurter, S.J., Johnson, J.R., 1993. Heat flow from the Earth's interior: analysis of the global data set. Rev. Geophys. 31 (3), 267–280.
Redi, M.H., 1982. Oceanic isopycnal mixing by coordinate rotation. J. Phys. Oceanogr. 12 (10), 1154–1158.
Sclater, J.G., Jaupart, C., Galson, D., 1980. The heat flow through oceanic and continental crust and the heat loss of the earth. Rev. Geophys. 18 (1), 269–311.
Scott, J.R., Marotzke, J., Adcroft, A., 2001. Geothermal heating and its influence on the meridional overturning circulation. J. Geophys. Res. Oceans 106 (C12), 31141–31154.
Speer, K.G., 1989. The stommel and arons model and geothermal heating in the south pacific. Earth Planet. Sci. Lett. 95 (3–4), 359–366.
Stein, C.A., Stein, S., 1992. A model for the global variation in oceanic depth and heat flow with lithospheric age. Nature 359 (6391), 123–129.
Stein, C.A., Stein, S., 1994. Constraints on hydrothermal heat flux through the oceanic lithosphere from global heat flow. J. Geophys. Res. Solid Earth 99 (B2), 3081–3095.
Stommel, H., 1982. Is the south pacific helium-3 plume dynamically active? Earth Planet. Sci. Lett. 61 (1), 63–67.
Thompson, L., Johnson, G.C., 1996. Abyssal currents generated by diffusion and geothermal heating over rises. Deep Sea Res. Part I 43 (2), 193–211.
Urakawa, L.S., Hasumi, H., 2009. A remote effect of geothermal heat on the global thermohaline circulation. J. Geophys. Res. Oceans 114 (C7).
Zalesak, S.T., 1979. Fully multidimensional flux-corrected transport algorithms for fluids. J. Comput. Phys. 31 (3), 335–362.
Zweng, M.M., et al., 2013. World Ocean Atlas 2013, Volume 2: Salinity. NOAA Atlas NESDIS 74.